RSC Advances

PAPER

View Article Online
View Journal | View Issue

Cite this: *RSC Adv.*, 2016, **6**, 33901

SBA-15 supported ionic liquid phase (SILP) with $H_2PW_{12}O_{40}^-$ for the hydrolytic catalysis of red macroalgal biomass to sugars†

Lenny B. Malihan, Grace M. Nisola, Neha Mittal, Seong-Poong Lee, Jeong Gil Seo, Hern Kim and Wook-Jin Chung*

Received 10th February 2016
Accepted 24th March 2016

DOI: 10.1039/c6ra03740b

www.rsc.org/advances

A supported ionic liquid phase (SILP) catalyst for biomass hydrolysis was prepared *via* immobilization of an acidic ionic liquid (IL) with a phosphotungstic counter-anion $H_2PW_{12}O_{40}^-$ (HPW) on ordered mesoporous silica (SBA-15). Characterization results from XRD, N_2 physisorption, FT-IR, TGA and SEM/TEM image analyses confirmed the successful preparation of the SILP catalyst (SBA-IL–HPW). Meanwhile, its catalytic performance was evaluated in terms of sugar production from the hydrolysis of different biomasses in water. Under optimal hydrolysis conditions, SBA-IL–HPW yielded 73% D-galactose from agarose and 58% D-glucose from cellobiose. Moreover, SBA-IL–HPW effectively hydrolyzed the red macroalgae *G. amansii* as it afforded 55% total reducing sugar and 38% D-galactose yields. SBA-IL–HPW was easily separated from the hydrolysates after reaction and was re-used five times without significant loss of activity. Overall findings reveal the potential of SBA-IL–HPW as a durable, environmentally benign catalyst for sugar production from renewable resources.

1. Introduction

Biomass have been widely utilized as renewable energy resources for the production of bio-fuel and bio-based chemicals. For example, lignocellulosic agricultural residues and forest woody feedstocks have already been employed as substrates for bio-ethanol production.[1] Aquatic biomasses such as *Laminaria*, *Saccorhiza*, *Alaria* and *Gelidium* have also shown potential as sugar resources due to their high carbohydrate contents. These macroalgal species are more viable than lignocellulosic materials because of their low lignin content, abundance and simple cultivation environment.[2]

Pretreatment strategies involving dilute or concentrated acids, enzymes and supercritical water have been utilized to enhance the digestibility of biomass substrates.[3] Recently, environmentally benign ionic liquids (IL) have been used to efficiently dissolve macroalgal biomass for their subsequent hydrolysis to sugars.[4,5] However, IL-based homogeneous catalysis has several drawbacks such as utilization of large amounts of expensive ILs, their complex recovery from the reaction mixture and possible mass transfer limitations due to their high viscosity.[6] In effect, only a small fraction of the IL is utilized and the reaction occurs only at the diffusion layer of the IL-catalyst phase rather than in the bulk phase.[7]

Supported ionic liquid phase (SILP) catalysis has been developed to address these issues. SILP materials are prepared by overlaying an IL film over a solid support with a high surface area. The resulting material appears as dry solid but up-close contains the active species as a thin liquid film in its pores.[8] SILP catalysts combine the benefits of high activity and selectivity from homogeneous catalysts with that of the recyclability, large surface area and hydrothermal stability of heterogeneous systems.[6] Various organic reactions such as hydroformylation,[9] esterification,[10] polymerization,[11] amination,[12] dehydration[6] and metal scavenging systems[13] have already been performed using SILP catalysts. In biomass pretreatment, SILP catalysts bearing Brønsted acidic groups could be more advantageous since they can effectively hydrolyze the biomass and be re-used multiple times. Acidic counter-anions such as HSO_4^- anion[6,14–16] and polyoxometalate species[17,18] have already been employed as SILP catalysts and used in various reactions. However, the use of SILP catalysts in biomass hydrolysis has been scarce. A sulfonic acid functionalized IL supported on silica gel was reported previously for the hydrolysis of cellulose using 1-*n*-butyl-3-methylimidazolium chloride ([BMIM]Cl) as solvent.[19] But the use of a large amount of IL as solvent during hydrolysis would not make this system economically feasible.

Heteropolyacids (HPAs) have been particularly used in cellulose hydrolysis[20,21] due to their strong acidity making them promising IL counter-anions. Among the Keggin HPAs, phosphotungstic acid ($H_3PW_{12}O_{40}$, HPW) has the highest acidity

Energy and Environment Fusion Technology Center (E^2FTC), Department of Energy Science and Technology (DEST), Myongji University, 116 Myongji-ro, Cheoin-gu, Yongin City, Gyeonggido 17058, South Korea. E-mail: wjc0828@gmail.com; Fax: +82-31-337-2902; Tel: +82-31-330-6687

† Electronic supplementary information (ESI) available. See DOI: 10.1039/c6ra03740b

approaching the superacid region. In fact, HPW exhibits stronger acidity as compared to mineral acids (*e.g.* H_2SO_4, HNO_3 and HCl) as evidenced by its low deprotonation enthalpy from density functional theory calculations.[21] Meanwhile, the mesoporosity of SBA-15 (2–50 nm) and its large surface area (500–1000 $m^2\ g^{-1}$) could facilitate convenient diffusion of large substrate molecules while its thick walls (3.1–6.4 nm) make it a thermally stable support. Moreover, it has abundant silanol groups available for functionalization.[22]

Herein, an HPW-based acidic ionic liquid anchored on ordered mesoporous SBA-15 (SBA-IL–HPW) was synthesized and used as an SILP catalyst for the hydrolysis of several types of biomasses for sugar production. The SILP catalyst was extensively characterized by X-ray diffraction (XRD), N_2 adsorption–desorption, thermogravimetric analysis (TGA), Fourier transform-infrared (FT-IR) spectroscopy, scanning electron microscopy (SEM) and transmission electron microscopy (TEM) to confirm its successful preparation. The applicability of SBA-IL–HPW for sugar production was investigated *via* hydrolysis of agarose, cellobiose and a red macroalgae, *Gelidium amansii*. Moreover, the long term hydrothermal stability of the catalyst was studied through a series of hydrolytic cycles.

2. Experimental

2.1 Materials

All chemicals were of analytical grade and were used as received. Poly(ethylene oxide)–poly(propylene oxide) or Pluronic® 123 (average molecular weight = 5800 g mol^{-1}), 3-chloropropyl-triethoxysilane (CPTES), toluene (anhydrous, 99.8%) were purchased from Sigma Aldrich (USA). Tetraethyl orthosilicate (TEOS, 98%), *N*-methylimidazole, *n*-butylamine and the heteropolyacid hydrate of $H_3PW_{12}O_{40}$ were procured from Acros Organics (Belgium). Hydrochloric acid (37% HCl) was from Showa (Japan). Agarose, glucose and galactose were supplied by Acros Organics (Belgium), whereas cellobiose was from Sigma Aldrich (USA).

Dried *Gelidium amansii* was supplied by Natural Food (http://0808.or.kr) from Sanjeong-dong, Mokpo, South Korea. Samples were washed with deionized (DI) water to remove residual salts and dried at 40 °C until the moisture content was ≤10 wt%. The dried samples were pulverized and stored in a desiccator when not in use.

2.2 Catalyst synthesis

2.2.1 Preparation of mesoporous SBA-15. Ordered mesoporous silica SBA-15 was synthesized according to methods reported elsewhere[23] using tri-block copolymer Pluronic® 123 as a structure directing agent. Approximately 10 g of Pluronic® 123 was dissolved in 325 mL of DI water and 60 mL of HCl at 40 °C. After dissolution, 20.6 g of TEOS was added and stirred for 2 h at 800 rpm. The suspension was statically aged in an oven at 40 °C for 24 h and further at 80 °C for another 24 h. The produced SBA-15 was repeatedly washed with hot (80 °C) DI water and dried at room temperature for 4 days followed by calcination at 500 °C in air (2.5 °C min^{-1}) for 5 h. Prior functionalization, SBA-15 was activated at 80 °C *in vacuo* for 4 hours.

2.2.2 Synthesis of SBA-IL. The IL, 1-(tri-ethoxy-silyl-propyl)-3-methylimidazolium chloride, was prepared following a reported procedure.[24] In a typical reaction, 0.10 mol (8.21 g) of *N*-methylimidazole and 0.10 mol (24.08 g) of 3-chloropropyl-triethoxysilane were stirred at 95 °C for 24 h. The product was extracted twice with diethyl ether and dried at room temperature. Meanwhile, SBA-15 was functionalized with the IL according to a previous method.[24] In a typical reaction, 1.5 g of the synthesized IL was added to 3 g of vacuum-dried SBA-15 dispersed in 90 mL of anhydrous toluene. The mixture was stirred for 16 h at 90 °C under a nitrogen atmosphere. The functionalized SBA-15 was then filtered, washed with toluene and vacuum-dried at 50 °C for 12 h. Excess IL was removed by 24 h Soxhlet extraction using boiling dichloromethane followed by vacuum drying at 50 °C. The resulting material was designated as SBA-IL.

2.2.3 Immobilization of HPW onto SBA-IL (SBA-IL–HPW). The SILP catalyst was obtained *via* anion exchange of 1 mmol HPW with 1 g of vacuum-dried (80 °C, 1 h) SBA-IL. HPW was initially dissolved in 50 mL DI water before addition of SBA-IL. The dispersion was stirred for 12 h at room temperature. After the reaction, the solid product was filtered off, washed with DI water (4 × 25 mL) to remove the residual HPW and further dried at 50 °C *in vacuo* for 24 h. The resulting SILP material was designated as SBA-IL–HPW.

2.3 Catalyst characterization

Low angle XRD patterns were measured in a PANalytical EMPYREAN SWAX diffractometer operated at 40 kV and 25 mA, calibrated with a standard silicon sample using Ni-filtered Cu-Kα (λ = 0.15406 nm) within 0.3–10° 2θ range. Wide angle powder XRD patterns were acquired using PANalytical, X'Pert-Pro diffractometer with Cu-Kα radiation operated at 40 mA and 40 kV with 0.03° step size in the 2θ range of 5–50°. Nitrogen adsorption–desorption isotherms were obtained using a Belsorp-mini II (Bel Japan, Inc.) system at 77 K. The samples were degassed under vacuum at 60 °C for 2 h prior measurements. The specific surface area of the samples was calculated using the Brunauer–Emmett–Teller (BET) method using the adsorption isotherms acquired at P/P_0 = 0.05–0.15. The pore volume and pore diameter were determined *via* Barrett–Joyner–Halenda (BJH) method from the adsorption branch of the isotherms. Mean pore size was obtained from the maximum BJH pore size distributions. The morphology of the samples was examined under Hitachi S-3500 N SEM and field emission TEM (JEOL, JEM-2000EX) operated at 200 kV. FT-IR spectra of the samples were recorded on a VARIAN FTS 2000 (Scimitar Series) FT-IR spectrophotometer using anhydrous KBr as standard (1 wt% of the sample). The tungsten (W) content in SBA-IL–HPW was determined using inductively coupled plasma-atomic emission spectroscopy (ICP-AES). Thermogravimetric analysis (TGA) was carried out on a Mettler Toledo (DSC823e) analyzer operated from 35 °C to 1000 °C with a heating rate of 10 °C min^{-1} in N_2, supplied at 50 mL min^{-1}. The acidic strength and

acid sites of the catalyst were quantified by potentiometric titration with 0.05 M *n*-butylamine in acetonitrile using a TitroLine® 7000 system from SI analytics. Initial electrode potential (E_i) indicates the maximum acid strength of the sample which is classified as: $E_i > 100$ mV (very strong acid sites), $0 < E_i < 100$ mV (strong sites), $-100 < E_i < 0$ mV (weak sites) and $E_i < -100$ (very weak sites).[25] The total number of acid sites present in the solid sample was determined at the equivalence point (mmol amine per g catalyst).

2.4 Biomass hydrolysis

The hydrolytic activity of the SILP catalyst was evaluated using substrate models such as agarose and cellobiose and a red macroalgae, *G. amansii*. All experiments were carried out in a Teflon-lined steel autoclave reactor. In a typical reaction, a mixture of 1 wt% biomass suspension in water and known amount of SBA-IL–HPW were placed in the reactor. The sample was stirred briefly at room temperature. The reactor was then placed in an oven at a specified temperature and time. The reaction was quenched by rapidly cooling the reactor in an ice bath and the catalyst was retrieved by centrifugation. The sugar content in the supernatant was analyzed as detailed in Section 2.5. For the hydrolysis of *G. amansii*, its initial sugar composition was determined using a modified two-step acid hydrolysis described previously.[5] Compositional analysis showed a glucose and galactose content of 18.14 and 28.48 wt%, respectively. Sugar yields were calculated based on this initial carbohydrate content. The total reducing sugar in *G. amansii* hydrolysates were calculated based on the total glucose and galactose content of 46.62 wt%.

2.5 Analysis of products and quantification of sugar yields

Total reducing sugars (TRS) were quantified using the DNS method described elsewhere.[26] The TRS concentration (C_{TRS}) of *G. amansii* hydrolysates was calculated based on a standard curve obtained with glucose. The concentration of monosaccharides and other reaction products (C_{HPLC}) were quantified using High Performance Liquid Chromatography (HPLC) equipped with a Refractive Index Detector (HPLC-RID) and a Biorad Aminex HPX-87H Ion Exclusion Column (300 mm × 7.8 mm). Column and detector temperatures were kept at 60 and 40 °C, respectively. The 5 mM H_2SO_4 mobile phase was filtered, degassed and delivered at 0.6 mL min^{-1}. The mass of TRS (M_{TRS}) was calculated using eqn (1) whereas that of the monosaccharides (M_{sugar}) was calculated using eqn (2) wherein V_1 is the volume of the solution. Sugar yields were calculated using eqn (3) given the mass of agarose (M_A), cellobiose (M_C) and *G. amansii* (M_{GA}) where *A* is the individual sugar content in the red macroalgae. Galactose yields from agarose were calculated by multiplying M_A with 0.5 assuming it contains equimolar amounts of galactose and 3,6-anhydro-L-galactose (3,6-AHG). Reported sugar yields are average values of at least duplicate runs.

$$M_{TRS}(\text{mg}) = C_{TRS}\left(\text{mg mL}^{-1}\right) \times \left(\frac{5}{0.5}\right) \times V_1(\text{mL}) \quad (1)$$

$$M_{sugar}\ (\text{mg}) = C_{HPLC}\ (\text{mg mL}^{-1}) \times V_1\ (\text{mL}) \quad (2)$$

$$\text{Yield}\ (\text{wt\%}) = \frac{M_{sugar}\ \text{or}\ M_{TRS}}{(M_A \times 0.5)\ \text{or}\ M_C\ \text{or}\ (M_{GA} \times A)} \times 100 \quad (3)$$

2.6 Recycling of the catalyst

After each hydrolysis run, SBA-IL–HPW was separated from the reaction mixture by centrifugation at 4000 rpm for 10 min. The retrieved SILP was washed with DI water and dried at 60 °C *in vacuo* for 24 h prior re-use.

2.7 Stability of the catalyst

A modified hot filtration experiment was performed as a leaching test to investigate the stability of the SILP catalyst during hydrolysis.[27] A pre-weighed sample of SBA-IL–HPW SILP was autoclaved several cycles in DI water. For each leaching cycle, fresh water was used; the SILP was separated from the water *via* gravity filtration using a filter paper. The autoclaved water, collected from each cycle, was loaded with agarose and then re-autoclaved for the hydrolysis reaction. Samples were collected and galactose yields were quantified as detailed in Section 2.5. High galactose yield would suggest elution of HPW into the water from the SILP.

3. Results and discussion

3.1 Synthesis of the catalyst

The SBA-IL–HPW SILP catalyst was prepared by covalent attachment of the pre-synthesized chloride-containing IL on mesoporous SBA-15 (Scheme 1). This method avoids the destruction of the support material in contrast to immobilization *via* the anion and decreases the possible leaching of the active sites.[24] Under benign reaction conditions, the acid sites were created on SBA-IL by anion exchange between chloride and $H_3PW_{12}O_{40}$ to afford the SILP catalyst. The successful preparation of SBA-IL–HPW was determined through a series of characterization techniques discussed in Section 3.2.

3.2 Characterization of the prepared catalysts

3.2.1 Structural and morphological properties. Low angle XRD patterns of pristine SBA-15 (Fig. 1) revealed three well-resolved peaks at $2\theta = 0.88°$, 1.54° and 1.78°, which can be indexed as (1 0 0) (strong), (1 1 0) (weak) and (2 0 0) (weak), respectively. These peaks are characteristic of hexagonal (*p6mm*) SBA-15 which has a significant degree of long-range order and a well-formed two dimensional meso-structure.[28] IL modification (SBA-IL) and further incorporation of the heteropolyacid (SBA-IL–HPW) exhibited lower peak intensities especially with the (1 0 0) signal. This is indicative of pore-filling effect in SBA-15 which is consistent with the increased wall thickness (Table 1) of both modified SBA-15 samples. Diffraction peaks at higher 2θ degrees were still evident in the functionalized materials (inset Fig. 1) albeit at lower intensities. This suggests

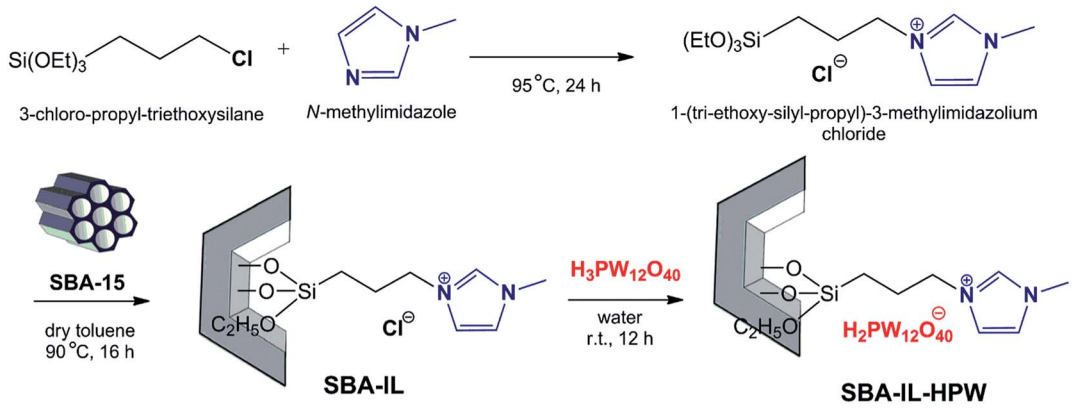

Scheme 1 Reaction scheme for the synthesis of SBA-IL–HPW.

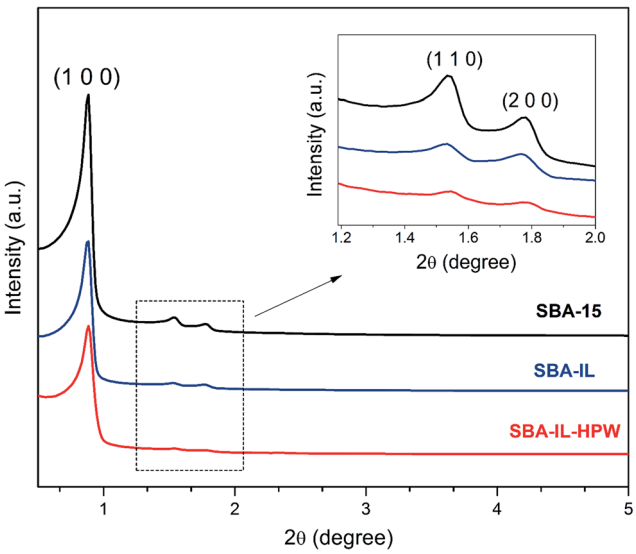

Fig. 1 Low angle XRD patterns of SBA-15, SBA-IL and SBA-IL–HPW.

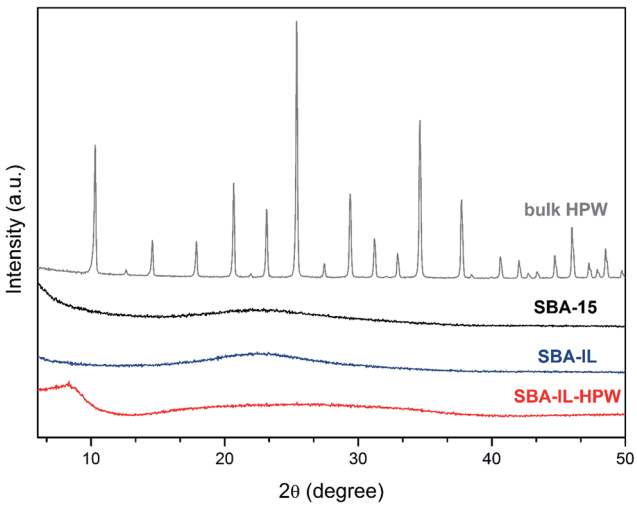

Fig. 2 Wide angle XRD patterns of bulk HPW, SBA-15, SBA-IL and SBA-IL–HPW.

an intact SBA-15 structure after immobilization, as further evidenced by the unaltered d_{100}-spacing = 9.9 nm in all samples.

To further observe the presence of HPW on SBA-15, Fig. 2 shows the wide angle XRD patterns for bulk HPW, SBA-15, SBA-IL and SBA-IL–HPW. SBA-15 revealed a broad band at 22.5° corresponding to amorphous silica. No considerable changes were observed when SBA-15 was functionalized with the IL (SBA-IL). The SILP catalyst, SBA-IL–HPW exhibited a similar pattern with a broad band centered at 25°. Compared with bulk HPW which showed various crystalline peaks, no prominent peaks related to the Keggin anion was observed in SBA-IL–HPW. This suggests that HPW were present as charge compensating anions of the IL and were not in their crystalline form.[27]

The mesoporosity of all SBA-based samples (Fig. 3A) was evidenced by the irreversible type IV N_2 adsorption–desorption

Table 1 Physico-chemical properties of SBA-15, SBA-IL and SBA-IL–HPW

Samples	Surface area[a] ($m^2\ g^{-1}$)	Pore volume[b] ($cm^3\ g^{-1}$)	Ave. pore diameter[c] (nm)	Wall thickness[d] (nm)
SBA-15	812	1.06	4.03	7.49
SBA-IL	366	0.63	3.53	7.99
SBA-IL–HPW	159	0.26	2.71	8.81

[a] Calculated by the BET equation at P/P_0 = 0.05–0.15. [b] BJH pore adsorption volume. [c] Adsorption average pore diameter. [d] Wall thickness = a_0 − pore size; $a_0 = 2d_{(100)}/\sqrt{3}$.[27]

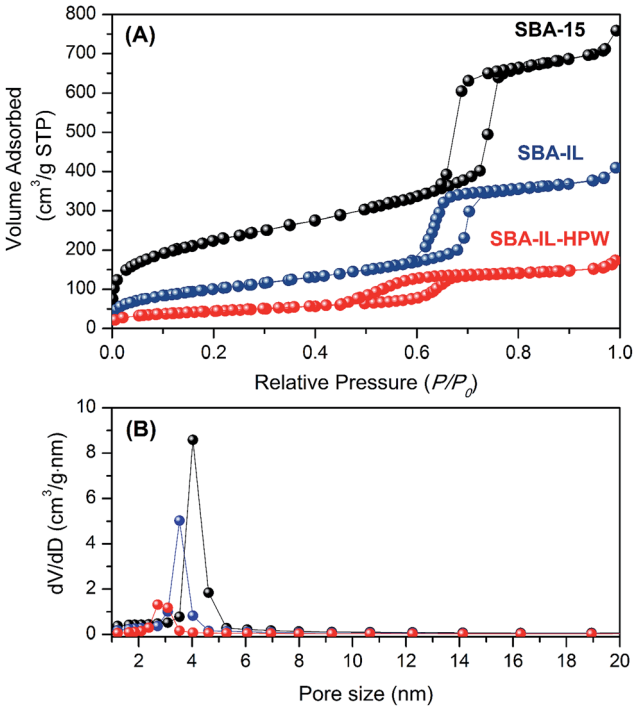

Fig. 3 N_2 adsorption–desorption isotherms (A) and pore size distribution curves (B) of SBA-15, SBA-IL and SBA-IL–HPW.

isotherms with H1-type hysteresis loops (as defined by IUPAC) associated with capillary condensation taking place in the channels. A wide hysteresis loop at $P/P_0 = 0.6$–0.8 was observed in SBA-15 while those in SBA-IL and SBA-IL–HPW shifted to a lower relative pressure which could be due to the coating and filling of the pores of SBA-15.[29]

From the N_2 adsorption–desorption curves, the structural properties of the samples including BET surface area and pore dimensions were acquired (Table 1). The surface area of SBA-15 (SA = 812 $m^2 g^{-1}$) decreased after IL functionalization (SA = 366 $m^2 g^{-1}$) and further upon anion exchange with HPW (SA = 159 $m^2 g^{-1}$). The presence of the acidic IL in SBA-IL–HPW was also evidenced by the decrease in pore volume (Table 1) and pore diameter (Fig. 3B). All the samples exhibited narrow pore size distributions indicating structural consistency before and after immobilization. The decrease in surface area and pore volume, together with the increase in wall thickness of SBA-15 confirmed the successful incorporation of the acidic IL in its pores.

The morphologies of bare SBA-15 and SBA-IL–HPW were examined by SEM (Fig. 4). SBA-15 exhibited wavy or rope-like mesopore domains (Fig. 4a), which aggregated into a wheat-like structure.[30] SBA-IL–HPW (Fig. 4b) showed similar morphology with its parent support but TEM images reveal the difference between the samples. Pristine SBA-15 (Fig. 4e) exhibited highly ordered hexagonal meso-structure whereas an amorphous IL layer (inset: Fig. 4f) was evident on the surface of SBA-IL–HPW. This further confirms the successful attachment of the acidic IL on SBA-15 and the formation of an SILP material.

3.2.2 Surface chemical properties. FT-IR spectra (Fig. 5) of all samples confirmed the successful functionalization of SBA-15 with the IL and subsequent anion exchange with HPW. Pristine SBA-15 featured the symmetric and asymmetric stretching of Si–O–Si bands at 806 and 1000–1200 cm^{-1},

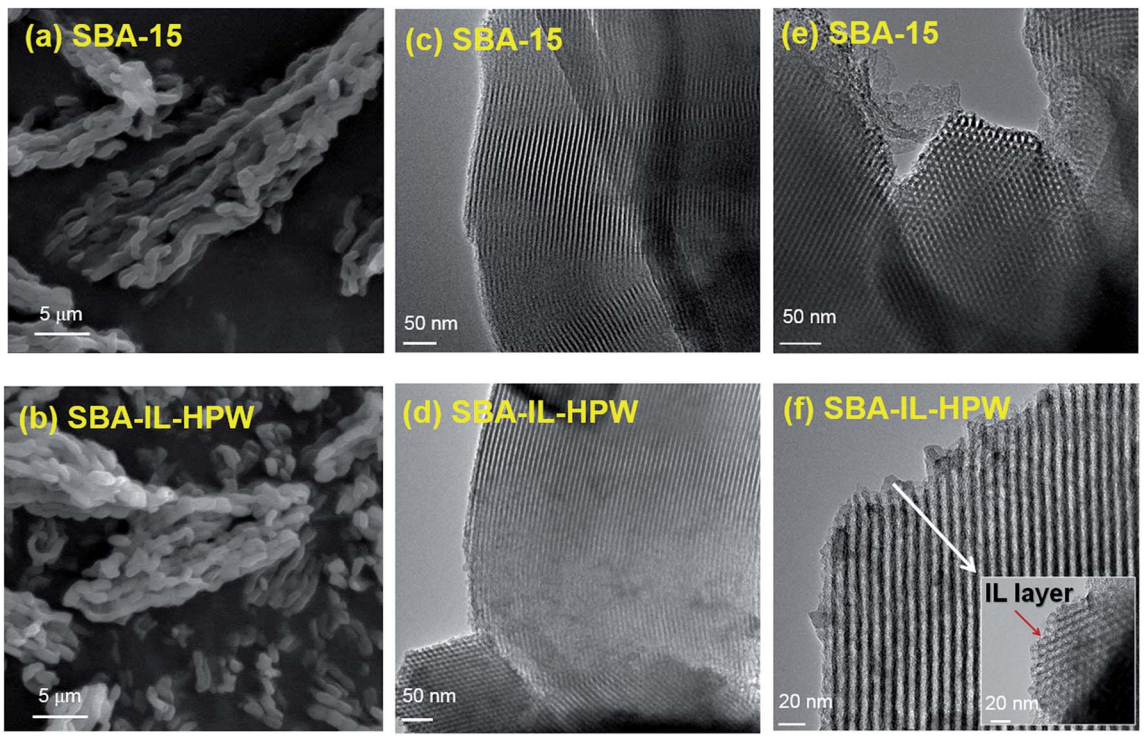

Fig. 4 SEM images of (a) SBA-15 and (b) SBA-IL–HPW; TEM images of SBA-15 (c and e) and SBA-IL–HPW (d and f).

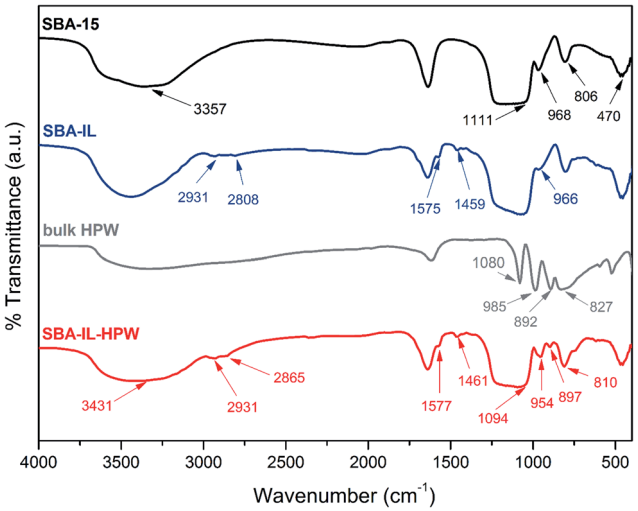

Fig. 5 FT-IR spectra of SBA-15, SBA-IL, bulk HPW and SBA-IL–HPW.

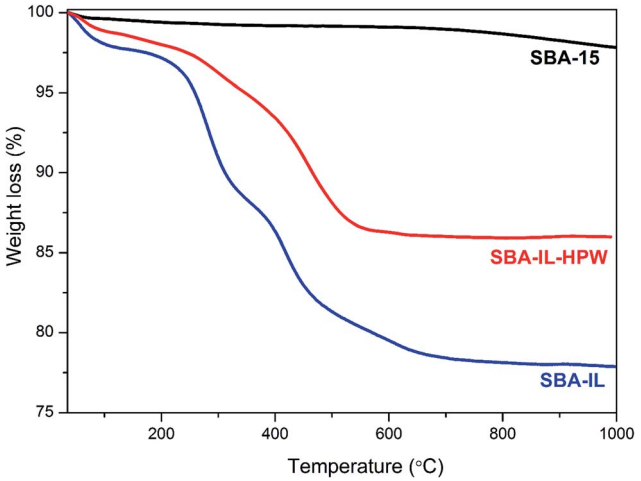

Fig. 6 Thermogravimetric curves of SBA-15, SBA-IL and SBA-IL–HPW.

respectively. The stretching vibrations of terminal ≡Si–OH in SBA-15 is evident at 968 cm^{-1} while the bending vibrations of the Si–O unit could be observed at 470 cm^{-1}.[31] The peak at 3357 cm^{-1} could be due to OH– stretching of silanols and adsorbed water. Characteristic peaks in SBA-IL confirmed the successful binding of the IL on the silica support. The lower absorbance at 966 cm^{-1} in SBA-IL could be due to the interaction of the ethoxy groups from the IL with the surface silanols in SBA-15. Moreover, the presence of peaks at 1459 and 1575 cm^{-1} in SBA-IL could be attributed to the presence of the C=N and aromatic C=C stretching of the imidazolium cation, respectively. The weak bands at 2931 and 2808 cm^{-1} are due to the methylene vibrations of the propyl chain in the organosilane moiety.[10,31,32] The structure of $PW_{12}O_{40}^{3-}$ consists of a PO_4 tetrahedron surrounded by four W_3O_{13} groups which are connected by corner-sharing oxygens. Bulk HPW features four characteristic bands at *ca.* 1080, 985, 892 and 827 cm^{-1}, attributable to the asymmetric stretching of P–O, terminal W=O, corner-sharing W–O_c–W and edge-sharing W–O_b–W bonds, respectively.[33] Though most of the characteristic peaks of HPW were masked in the spectra due to the strong absorption bands of silica, the presence of W–O–W band at 897 cm^{-1} and the higher intensity of the band at 954 cm^{-1} suggest the presence of HPW in SBA-IL–HPW. Moreover, ICP-AES analysis of SBA-IL–HPW revealed an estimated W content of 2158 ppm (*i.e.* 0.98 μmol g^{-1} HPW). These findings further assert the successful immobilization of the acidic IL onto SBA-15, an SILP acidic catalyst.

3.2.3 Thermal stability. Thermal gravimetric curves of bare and functionalized SBA-15 (Fig. 6) reveal weight losses at temperature ≤ 100 °C, which can be ascribed to the removal of moisture and residual solvents. Among the samples, pristine SBA-15 exhibited the least overall weight loss of 1.35 wt% at >600 °C due to the condensation of surface silanols to siloxanes. The presence of the IL moiety explains the higher weight reduction in SBA-IL. The gradual weight decline (19.77%) at 150–700 °C was mainly due to the decomposition of the IL which is equivalent to 0.61 mmol g^{-1} IL on SBA-15. Meanwhile, SBA-IL–HPW showed an overall weight loss of 12.72%. The weight loss at $T > 300$ °C can be ascribed to the decomposition of the cation as well as partial loss of the heteropolyacid.[34] The lower weight loss in SBA-IL–HPW than in SBA-IL is mainly due to the addition of inorganic and relatively more thermally stable HPW. DTG curve of SBA-IL–HPW (Fig. S1†) showed the rapid loss of the acidic IL from 280–460 °C. Hence, the catalyst is thermally stable at temperatures below 280 °C.

3.2.4 Acidity of SBA-IL–HPW. SBA-15 exhibited very weak acid sites having an initial electrode potential (E_i) of −130.0 mV. On the other hand, SBA-IL–HPW exhibited very strong acid sites having an E_i of +120.8 mV corresponding to 0.1649 mmol g^{-1} (Fig. S2†).

3.3 Catalytic activity of SBA-IL–HPW

The catalytic activity of SBA-IL–HPW was demonstrated in the hydrolysis of red macroalgae and its representative model compounds: agarose and cellobiose using water as the solvent. Control hydrolysis runs with 50 mg of agarose in an autoclave for 12 h at $T = 120$ °C in the presence of SBA-15 and SBA-IL yielded solidified samples when cooled to room temperature. This suggests that both materials were unable to depolymerize and hydrolyze the substrate. These findings verify that neither material had active acidic sites which could catalyze agarose hydrolysis. Meanwhile, galactose yields of 80% from agarose and 56% from *G. amansii* were obtained from the hydrolysates in aqueous systems loaded with pure HPA (acid concentration = 1.98 mmol L^{-1}). This result confirms that, as the anionic form of HPA, HPW would be the sole active component in the SBA-IL–HPW SILP that would be responsible for the acidic hydrolysis of the substrates.

3.3.1 Effect of catalyst amount on agarose hydrolysis. The effect of catalyst amount on sugar yields was evaluated using agarose as a substrate which contains equimolar repeating units of α-(1,3)-D-galactose and β-(1,4)-3,6-anhydro-L-galactose.[35] A representative hydrolysis temperature of 120 °C was adapted for agarose based on a previous study.[5]

Table 2 Galactose yields (wt%) from the hydrolysis of agarose using different amounts of SBA-IL–HPW[a]

Entry	Catalyst amount (mg)	Galactose yield (wt%)
1	0	0
2	20	39.7
3	40	65.4
4	60	69.6
5	80	56.0
6	120	49.7

[a] Reaction conditions: 50 mg agarose, 5 mL DI water, autoclaved for 6 h at 120 °C.

Table 2 shows the D-galactose yields from the hydrolysis of agarose by varying the amount of SBA-IL–HPW. An increase in the sugar production concurrent with the increase in SBA-IL–HPW was observed. A maximum galactose yield of 70% was achieved with 60 mg of SBA-IL–HPW after 6 h. Further increase in SBA-IL–HPW reduced the galactose yield which can be ascribed to the formation of degradation compounds due to increased acidity in the system. Thus, 60 mg of SBA-IL–HPW was utilized for subsequent reactions unless otherwise stated.

3.3.2 Effect of reaction time on biomass hydrolysis. The hydrolysis performance of SBA-IL–HPW was further evaluated using cellobiose and a red macroalgae, *G. amansii*. Cellobiose, a sub-unit of cellulose, is a disaccharide with β-1,4-linked glucose units.[36] Meanwhile, the primary polysaccharides in *G. amansii* are fibrin (cellulose) and agarose.[37] Hydrolysis of cellobiose was carried out at a slightly higher temperature (*i.e.* 140 °C) as compared with agarose and *G. amansii* (*i.e.* 120 °C). The higher temperature requirement was due to the presence of β-1,4 linkages in cellobiose which are not readily hydrolyzed as compared with the α-linkages found in agarose.[38]

The acid-catalyzed hydrolysis of red macroalgal polysaccharides has been modeled as a pseudo-first order sequential reaction releasing sugars as galactose or glucose from the tested substrates, followed by sugar degradation (Scheme 2).[5] Extreme reaction conditions such as high acidity, prolonged reaction time and high hydrolysis temperature may drive the reaction towards the formation of degradation products such as 5-HMF, formic acid and levulinic acid.[39] Fig. 7A shows the galactose yields from the hydrolysis of agarose. Maximum galactose yield (73 wt%) was observed after 12 h of reaction, which plateaued at 71% after 24 h. The main decomposition product of agarose hydrolysis was 5-HMF (Table S1†) which started to form after 6 h of the reaction. This could be due to the hydrolysis of the acid labile 3,6-AHG, the other major component of agarose.[40] The yield of 5-HMF decreased after 24 h of reaction due to the formation of its re-hydration products such as formic and levulinic acids.[41]

Glucose yields from the hydrolysis of cellobiose were found to be maximum after 12 h of reaction (Fig. 7B). The highest glucose yield of 58% was released from cellobiose which declined to 33% after 24 h. The presence of decomposition products such as formic acid and 5-HMF were observed after 18 h of reaction (Table S2†). While glucose production declined, cellobiose attained ~99% conversion after 24 h, which suggests formation of sugar degradation products specifically levulinic acid (275.84 mg g^{-1} cellobiose) from the released glucose. The higher galactose yield from agarose has been consistent with previous reports as it is more acid-labile than substrates containing β-linkages such as cellulose or cellobiose.[5] A similar trend was observed in the hydrolysis of *G. amansii* (Fig. 7C) reaching a maximum galactose yield of 38% and a TRS yield of 58% after 12 h. There was no considerable increase in the sugar yields when the reaction was extended until 24 h. The main decomposition products formed during *G. amansii* hydrolysis are 5-HMF and formic acid (Table S3†). Meanwhile, no levulinic acid was detected in the hydrolysates suggesting that the galactose released from the hydrolysis of agarose is more susceptible to degradation as compared to that of *G. amansii*. Moreover, the absence of glucose from the hydrolysis of *G. amansii* has also been observed in earlier reports which involved

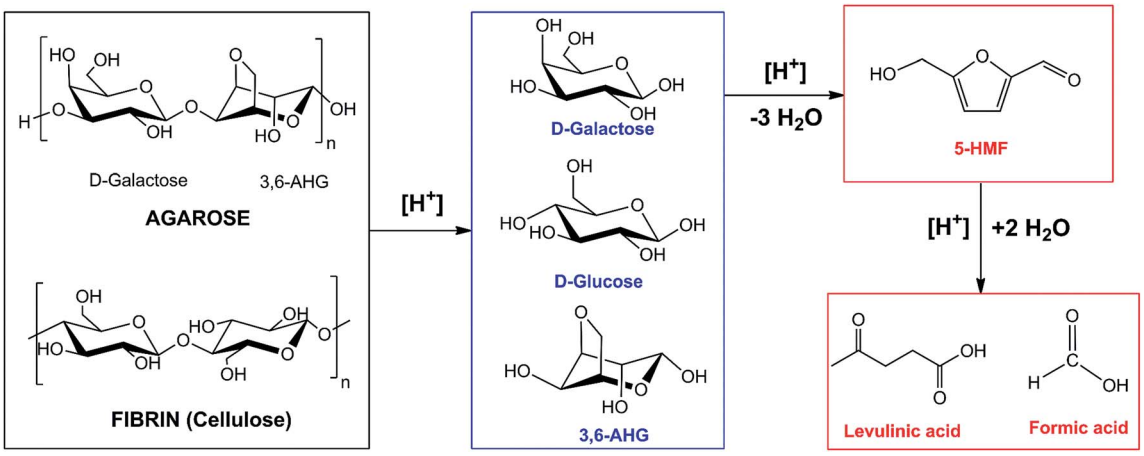

Scheme 2 Putative mechanism of acid-catalyzed hydrolysis of red macroalgal polysaccharides for sugar production and subsequent formation of degradation products using Brønsted acid catalysts.

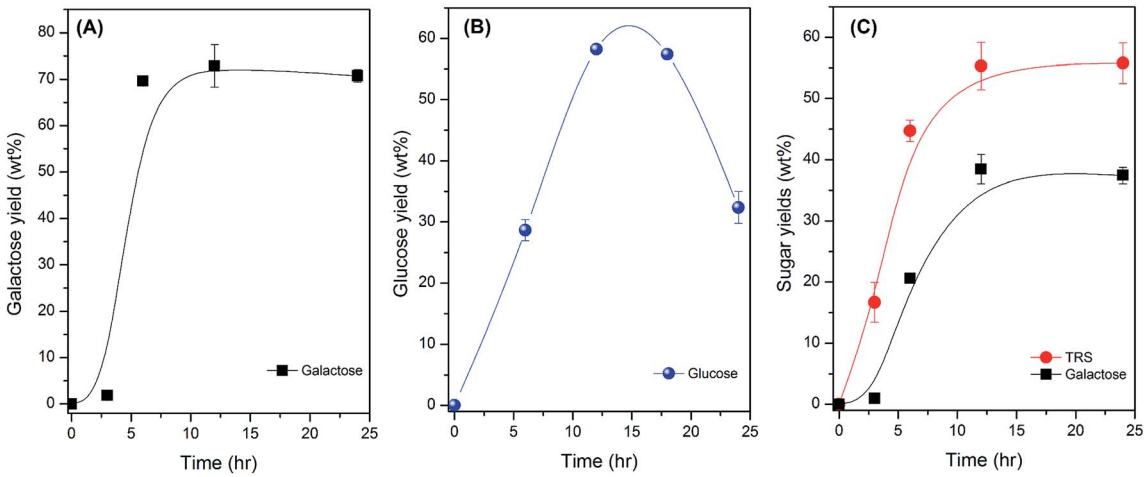

Fig. 7 Sugar yields (wt%) from the hydrolysis of agarose (A), cellobiose (B) and *G. amansii* (C) using SBA-IL–HPW at different time intervals. Reaction conditions: 50 mg substrate, 60 mg SBA-IL–HPW, 5 mL DI water, 120 °C for agarose and *G. amansii*, 140 °C for cellobiose, autoclave.

thermal acid hydrolysis systems since the polysaccharide present in this macroalgae is cellulose, which is more resistant than cellobiose.[42]

3.4 Re-usability and stability of SBA-IL–HPW

The hydrothermal stability of SBA-IL–HPW was demonstrated using the optimal conditions in the hydrolysis of agarose, *i.e.* 12 h at 120 °C. The catalyst was easily recovered after each hydrolysis reaction by centrifugation and re-used without further activation. Cycled experiment (Fig. 8) reveal a consistent performance (>70%) except after the second cycle, which showed a slightly higher galactose yield. Result from the modified hot filtration test (Table S5†) was consistent with this finding as the galactose yield in autoclaved water system (leaching solvent) was also highest (13%) at the first leaching cycle (Table S4†). These findings suggest that the increase of galactose yield at cycle 2 (Fig. 8) was due to the release of loosely bound HPW residuals from the SILP. The steady performance of the SILP in the succeeding hydrolytic cycles (Fig. 8) also agrees with the leaching test; the meager galactose yields at the latter cycles (Table S4†) suggest that HPW was not further leached out from the SILP after the first leaching cycle. In this regard, the temporary elution of HPW (after first hydrolytic run) had no significant deteriorating effect on the long term performance of the SILP.

Moreover, inspection of used SBA-IL–HPW *via* FT-IR analysis (Fig. S3†) reveal no chemical alteration even after five hydrolytic cycles. This further confirms that majority of the HPW remained intact in the SILP. Overall results demonstrate the reusability and stability of SBA-IL–HPW, and its potential as a resilient SILP catalyst for biomass-based sugars production.

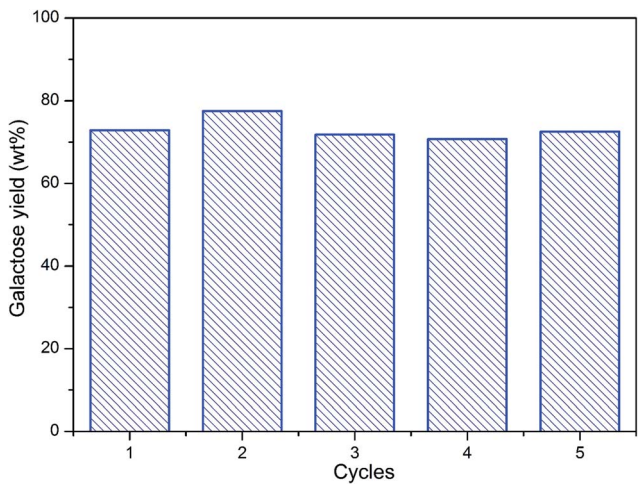

Fig. 8 Recyclability of SBA-IL–HPW in the hydrolysis of agarose. Reaction conditions: 50 mg agarose, 60 mg SBA-IL–HPW, 5 mL DI water, 120 °C, 12 h, autoclave.

4. Conclusions

Supported ionic liquid phase catalyst based on acidic HPW anion (SBA-IL–HPW) was successfully synthesized and applied for the hydrolysis of macroalgal biomass. Various characterization techniques confirmed that the acidic ionic liquid was covalently attached in the pores of ordered mesoporous SBA-15 rendering the SILP catalyst hydrothermally stable. The SILP catalyst effectively released sugars (*e.g.* galactose and glucose) from agarose, cellobiose and *G. amansii* with optimal sugar yields after 12 h of reaction. Moreover, SBA-IL–HPW could be easily recycled without significant loss of activity which makes it more industrially feasible as compared to homogeneous IL systems. Overall findings demonstrate the potential of SBA-IL–HPW as an SILP catalyst for biomass processing for sugar production.

Acknowledgements

This research was supported by Basic Science Research Program through the National Research Foundation of Korea (NRF)

funded by the Ministry of Education (2009-0093816) and by the Ministry of Science, ICT & Future Planning (No. 2015R1C1A2A01054605).

References

1 A. Limayem and S. C. Ricke, *Prog. Energy Combust. Sci.*, 2012, **38**, 449.
2 R. P. John, G. S. Anisha, L. Madhavan Nampoothiri and A. Pandey, *Bioresour. Technol.*, 2011, **102**, 186.
3 R. Kumar, S. Singh and O. V. Singh, *J. Ind. Microbiol. Biotechnol.*, 2008, **35**, 377.
4 L. B. Malihan, G. M. Nisola and W. J. Chung, *Bioresour. Technol.*, 2012, **118**, 545.
5 L. B. Malihan, G. M. Nisola, N. Mittal, J. G. Seo and W. J. Chung, *Renewable Energy*, 2014, **66**, 596.
6 K. B. Sidhpuria, A. L. Daniel-da-Silva, T. Trindade and J. A. P. Coutinho, *Green Chem.*, 2011, **13**, 340.
7 A. Riisager, R. Fehrmann, S. Flicker, R. van Hal, M. Haumann and P. Wasserscheid, *Angew. Chem., Int. Ed.*, 2005, **44**, 815.
8 R. Öchsner, M. J. Schneider, C. Meyer, M. Haumann and P. Wasserscheid, *Appl. Catal., A*, 2011, **399**, 35.
9 C. P. Mehnert, R. A. Cook, N. C. Dispenziere and M. Afeworki, *J. Am. Chem. Soc.*, 2002, **124**, 12932.
10 K. Qiao, H. Hagiwara and C. Yokoyama, *J. Mol. Catal. A: Chem.*, 2006, **246**, 65.
11 W. Ochędzan-Siodłak and K. Dziubek, *Appl. Catal., A*, 2014, **484**, 134.
12 A. H. Tamboli, A. A. Chaugule, F. A. Sheikh, W. J. Chung and H. Kim, *Chin. J. Catal.*, 2015, **36**, 1365.
13 W. Chen, Y. Zhang, L. Zhu, J. Lan, R. Xie and J. You, *J. Am. Chem. Soc.*, 2007, **129**, 13879.
14 J. Miao, H. Wan and G. Guan, *Catal. Commun.*, 2011, **12**, 353.
15 S. Rostamnia, A. Hassankhani, H. G. Hossieni, B. Gholipour and H. Xin, *J. Mol. Catal. A: Chem.*, 2014, **395**, 463.
16 Q. Zhang, J. Luo and Y. Wei, *Green Chem.*, 2010, **12**, 2246.
17 J. Kasai, Y. Nakagawa, S. Uchida, K. Yamaguchi and N. Mizuno, *Chem.–Eur. J.*, 2006, **12**, 4176.
18 J. Xiong, W. Zhu, W. Ding, L. Yang, M. Zhang, W. Jiang, Z. Zhao and H. Li, *RSC Adv.*, 2015, **5**, 16847.
19 A. S. Amarasekara and O. S. Owereh, *Catal. Commun.*, 2010, **11**, 1072.
20 J. Tian, J. Wang, S. Zhao, C. Jiang, X. Zhang and X. Wang, *Cellulose*, 2010, **17**, 587.
21 K. Shimizu, H. Furukawa, N. Kobayashi, Y. Itaya and A. Satsuma, *Green Chem.*, 2009, **11**, 1627.
22 B. Zou, Y. Hu, D. Yu, J. Xia, S. Tang, W. Liu and H. Huang, *Biochem. Eng. J.*, 2010, **53**, 150.
23 D. Zhao, J. Feng, Q. Huo, N. Melosh, G. H. Fredrickson, B. F. Chmelka and G. D. Stucky, *Science*, 1998, **279**, 548.
24 M. H. Valkenberg, C. de Castro and W. F. Hölderich, *Green Chem.*, 2002, **4**, 88.
25 A. S. Khder and A. I. Ahmed, *Appl. Catal., A*, 2009, **354**, 153.
26 C. Li and Z. K. Zhao, *Adv. Synth. Catal.*, 2007, **349**, 1847.
27 R. Gao, Q. Zhu, W. L. Dai and K. Fan, *RSC Adv.*, 2012, **2**, 6087.
28 N. Y. He, C. S. Woo, H. G. Kim and H. I. Lee, *Appl. Catal., A*, 2005, **281**, 167.
29 P. Krawiec, C. Weidenthaler and S. Kaskel, *Chem. Mater.*, 2004, **16**, 2869.
30 A. Lapkin, B. Bozkaya, T. Mays, L. Borello, K. Edler and B. Crittenden, *Catal. Today*, 2003, **81**, 611.
31 S. K. Kundu, J. Mondal and A. Bhaumik, *Dalton Trans.*, 2013, **42**, 10515.
32 L. T. Aany Sofia, A. Krishnan, M. Sankar, N. K. Kala Raj, P. Manikandan, P. R. Rajamohanan and T. G. Ajithkumar, *J. Phys. Chem. C*, 2009, **113**, 21114.
33 X. Han, W. Yan, K. Chen, C. T. Hung, L. L. Liu, P. H. Wu, S. J. Huang and S. B. Liu, *Appl. Catal., A*, 2014, **485**, 149.
34 S. Choi, Y. Wang, Z. Nie, J. Liu and C. H. F. Peden, *Catal. Today*, 2000, **55**, 117.
35 C. N. Jol, T. G. Neiss, B. Penninkhof, B. Rudolph and G. A. De Ruiter, *Anal. Biochem.*, 1999, **268**, 213.
36 J. A. Bootsma and B. H. Shanks, *Appl. Catal., A*, 2007, **327**, 44.
37 Y. Kim, D. Kim, T. Kim, M. K. Shin, Y. J. Kim, J. J. Yoon and I. S. Chang, *Biomass Bioenergy*, 2013, **56**, 38.
38 M. Kitano, D. Yamaguchi, S. Suganuma, K. Nakajima, H. Kato, S. Hayashi and M. Hara, *Langmuir*, 2009, **25**, 5068.
39 N. Mittal, G. M. Nisola and W. J. Chung, *Tetrahedron Lett.*, 2012, **53**, 3149.
40 B. Kim, J. Jeong, S. Shin, D. Lee, S. Kim, H. J. Yoon and J. K. Cho, *ChemSusChem*, 2010, **3**, 1273.
41 T. S. Jeong, Y. S. Kim and K. K. Oh, *Bioresour. Technol.*, 2011, **102**, 10529.
42 H. Cho, C. H. Ra and S. K. Kim, *J. Microbiol. Biotechnol.*, 2014, **24**, 264.